Strong-Motion Records for Site-Specific Analysis

Article *in* Earthquake Spectra · August 2003

DOI: 10.1193/1.1598439

1 author:

Praveen K. Malhotra
StrongMotions Inc.
84 PUBLICATIONS **1,607** CITATIONS

SEE PROFILE

Strong-Motion Records for Site-Specific Analysis

Praveen K. Malhotra,[a] **M.EERI**

A procedure is presented to select and scale strong-motion records for site-specific analysis. The procedure matches records' smooth response spectra with the site response spectrum by scaling of the acceleration histories. The parameters defining the smooth spectrum of various records are computed and tabulated to allow easy selection of records. Hazard de-aggregation is used to identify closer and distant seismic events, which are simulated by the scaled ground motion histories. The procedure can also be used to obtain ground motion pairs in orthogonal directions for multidimensional dynamic response analyses. [DOI: 10.1193/1.1598439]

INTRODUCTION

Strong-motion records are used in dynamic response analyses of structural and soil systems. Widespread deployment of seismic instruments has led to a dramatic increase in the number of strong-motion records. However, the selection of suitable records for site-specific analyses continues to be difficult.

The site-specific strong-motion records can be obtained by the following procedure: (1) establish a site-specific response spectrum from probabilistic seismic hazard analysis (Cornell 1968, Reiter 1991), (2) identify controlling seismic events by de-aggregating the seismic hazard (McGuire 1995, Cramer and Petersen 1996, Harmsen and Frankel 2001), (3) estimate strong-motion duration for the controlling seismic events, and (4) search strong-motion databases for records which are compatible with the site-specific response spectrum and are of required duration. Searching strong-motion databases for spectrum-compatible records can be tedious if the records are not arranged in a systematic manner.

OBJECTIVE AND ORGANIZATION

The objective of this paper is to simplify the selection and scaling of strong-motion records for site-specific analyses. The paper is organized as follows:

1. The response spectrum and duration of many recorded ground motions are computed;
2. Smooth spectral shapes are fitted through the actual spectra by least-square method;

[a] FM Global Research, 1151 Boston-Providence Turnpike, P.O. Box 9102, Norwood, MA 02062-9102; E-mail: Praveen.Malhotra@FMGlobal.com

Earthquake Spectra, Volume 19, No. 3, pages 557–578, August 2003;

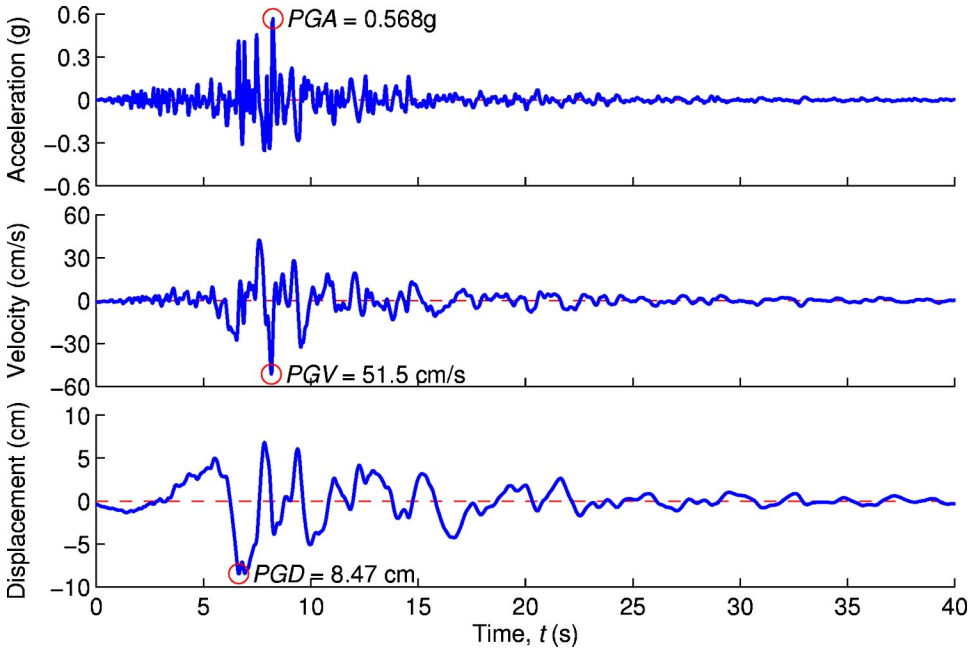

Figure 1. Processed acceleration, velocity, and displacement histories of ground motion recorded during the 1994 Northridge ($6.7M_w$), California, earthquake, at "Castaic Old Ridge Route" site (CSMIP Station No. 24278) in the 90° (east) direction. The data were downloaded from the CSMIP ftp site: ftp://ftp.consrv.ca.gov/pub/dmg/csmip.

3. The parameters defining the smooth spectrum and duration of various records are tabulated;
4. For an example site, the response spectrum is constructed from the results of probabilistic hazard analysis, dominant seismic events are identified and values of strong-motion duration estimated; and
5. A procedure is presented to select strong-motion records that can be scaled to achieve compatibility with site-response spectrum.

SMOOTH SPECTRUM OF RECORD

Figure 1 shows the processed acceleration, velocity, and displacement histories of horizontal motion recorded at a site, during the 1994 Northridge, California, earthquake. The site is identified as "Castaic Old Ridge Route" (Station No. 24278) by the California Strong Motion Instrumentation Program (CSMIP). The records were downloaded from the CSMIP ftp site: ftp://ftp.consrv.ca.gov/pub/dmg/csmip. The peak values of acceleration, velocity, and displacement in the 90° (east) direction are: $PGA = 0.568$ g, $PGV = 51.5$ cm/s, and $PGD = 8.47$ cm.

Figure 2 shows a tripartite plot of the 5% damped response spectrum of the Castaic 90° motion shown in Figure 1. In Figure 2, the pseudo-spectral velocity SV is read along

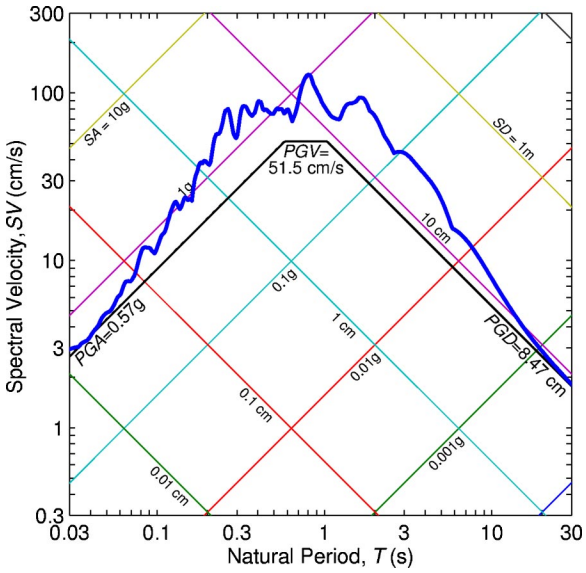

Figure 2. Tripartite response spectrum (5% damping) of the Castaic 90° ground motion shown in Figure 1.

the vertical axis, the pseudo-spectral acceleration SA along the −45° axis, and the spectral deformation SD along the +45° axis, with respect to the natural period T along the horizontal axis. These quantities are related to each other as follows (Newmark and Hall 1982, Chopra 2001):

$$SA \cdot \left(\frac{T}{2\pi}\right)^2 = SD = SV \cdot \left(\frac{T}{2\pi}\right) \tag{1}$$

In Figure 2, the peak values of ground acceleration, velocity, and displacement are shown by straight, dark lines. The response spectrum shows correct asymptotic behavior at both short and long periods—the spectral acceleration approaches PGA at short periods and the spectral deformation approaches PGD at long periods. This will not be the case if the response spectrum were computed from the acceleration history, which is not fully compatible with the displacement history. For the purpose of this study, the spectra were computed by the procedure described in Malhotra (2001), which ensures correct asymptotic behavior even when the processed acceleration, velocity, and displacement histories are not fully compatible with each other.

In Figure 3, the Newmark and Hall (1982) smooth spectrum is fitted through the actual spectrum by minimizing the sum-of-square error (difference) between the actual and the smooth spectrum. The Newmark-Hall smooth spectrum is defined by only nine parameters: PGA, $SA_{\max}$, control periods T_1 to T_6, and PGD.

The Newmark-Hall smooth spectrum is divided into three regions: (1) acceleration region $T<T_3$, (2) velocity region $T_3<T<T_4$, and (3) displacement region $T>T_4$ (Figure

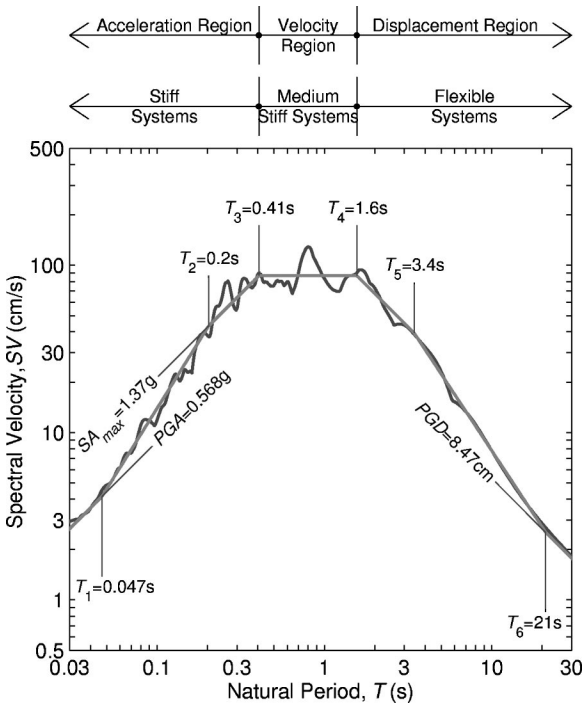

Figure 3. Smooth response spectrum (straight lines) fitted through the actual response spectrum (wavy line) of the Castaic 90° ground motion shown in Figure 1.

3). Systems with natural period in the acceleration region behave in a stiff manner—they experience small deformation and large force; systems with natural period in the displacement region behave in a flexible manner—they experience large deformation and small force; and systems with period in the velocity region behave in a medium-stiff manner. The control periods defining the boundaries of the acceleration, velocity, and displacement regions change from one ground motion to another. Therefore, it is possible for a given system to behave in a flexible manner for one ground motion and in a stiff manner for another (Malhotra 1999).

Considering that the natural period of most systems falls between T_2 and T_5, the smooth spectral shape can be simplified by extending the flat acceleration region to the left of T_2 and the flat displacement region to the right of T_5, as shown in Figure 4.

Figure 5 shows the linear plots of the actual (solid line) and the simplified smooth (dashed line) response spectra of the Castaic 90° ground motion. The simplified smooth spectrum is defined by just three parameters: $SA_{\max}$, T_3, and T_4. These are the key amplitude and frequency parameters of a ground motion, because they determine the amplitude of the load experienced by systems of different natural periods (or frequencies).

The $SA_{\max}$, T_3, and T_4 were computed for numerous ground motions. In Table 1 in the Appendix, they are arranged in ascending order of the control period T_3. The first

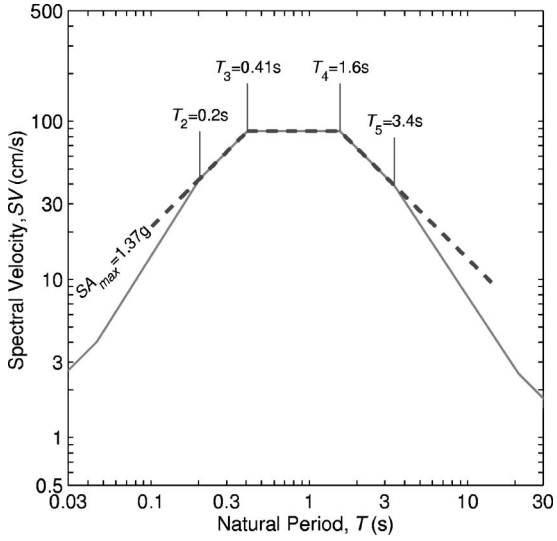

Figure 4. Smooth response spectrum (solid line) and the simplified smooth response spectrum (dashed line) of the Castaic 90° ground motion shown in Figure 1.

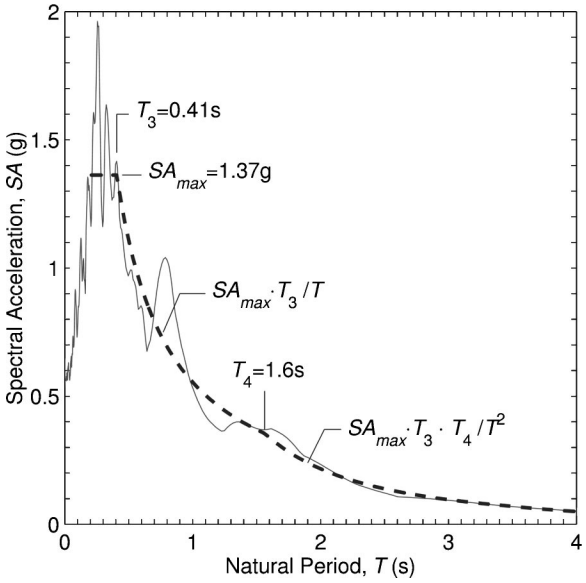

Figure 5. Linear plots of the actual (solid line) and simplified smooth (dashed line) response spectra of the Castaic 90° ground motion shown in Figure 1.

column in Table 1 identifies the station (site) at which the record was obtained and shows the direction of the recorded motion (measured clockwise from north). The second column identifies the name of the earthquake. Columns 3 to 5 show the values of SA_{max}, T_3, and T_4, respectively. Column 6 shows the duration of strong shaking (to be discussed later). Column 7 shows whether the record was from a soil (S) site or a rock (R) site. Column 7 shows the source (web site) from where the record was downloaded.

SIGNIFICANCE OF SA_{max}, T_3, AND T_4

The SA_{max} provides information regarding the high-frequency content of a ground motion. The higher the SA_{max}, the greater the amplitude of high frequencies in the ground motion. T_3 and T_4 provide information regarding the contribution of medium and low frequencies relative to the high frequencies in ground motion. In general, T_3 and T_4 are longer for soil sites compared to rock sites. T_3 and T_4 increase with increase in the size of the earthquake and increase in distance from the seismic source.

DURATION OF STRONG SHAKING

Whereas the amplitude and frequency distribution of a ground motion are captured by its response spectrum, its duration is not. We need to know the duration of strong shaking, because structures can fail in low cycle fatigue (Krawinkler et al. 1983) and saturated loose sandy soils can liquefy (Seed and Idriss 1982) when subjected to several load cycles during an earthquake (Kramer 1996). In the literature, there are more than 30 definitions of strong-motion duration (e.g., Bommer and Martinez-Pereira 1999), but they all are indirect measures of the number of load cycles. One of the more accepted definitions of duration is known as the significant duration. It is defined as the time difference between the arrivals of 5% and 95% of the area under the square of the acceleration history (Trifunac and Brady 1975). The significant duration for the Castaic 90° motion is D_s=9.1 s (see Figure 6). The significant durations for various ground motions are shown in the sixth column of Table 1.

SCALING OF RECORD

A simple way to modify a strong-motion record is to multiply the amplitude of the acceleration history throughout by a certain factor α. The record's *PGA*, *PGV*, and *PGD* all are multiplied by the factor α. The effect of scaling factor α=1.5 on the record's smooth response spectrum is shown in Figure 7. Note that SA_{max} increases by 50%, while the control periods T_3 and T_4 remain unchanged. The record's significant duration D_s is also not affected by scaling, because D_s depends on the shape, rather than the amplitude, of the record (Figure 6).

SITE-SPECIFIC SPECTRUM AND DURATION

The California Geological Survey (CGS) and the United States Geological Survey (USGS) have carried out probabilistic seismic hazard analyses of numerous sites within the United States, assuming firm rock site conditions (Petersen et al. 1996, Frankel et al. 1996). The results of these analyses have been used to generate the seismic hazard maps in building codes (Leyendecker et al. 2000).

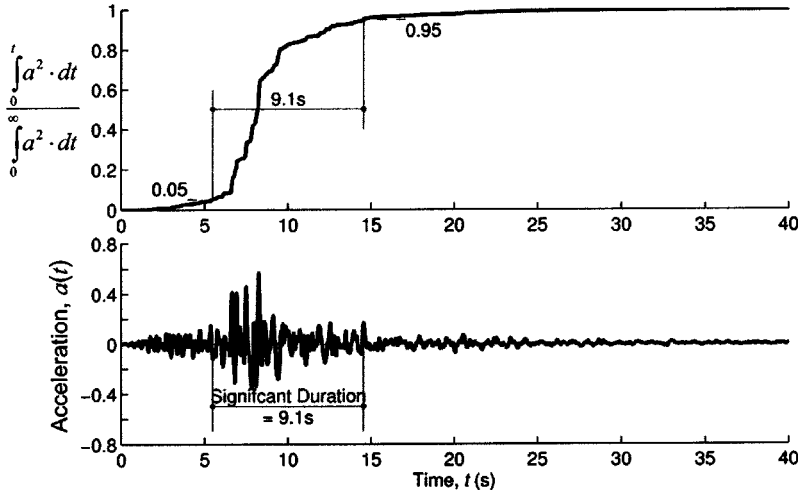

Figure 6. Significant-duration (Trifunac and Brady 1975) of the Castaic 90° ground motion shown in Figure 1.

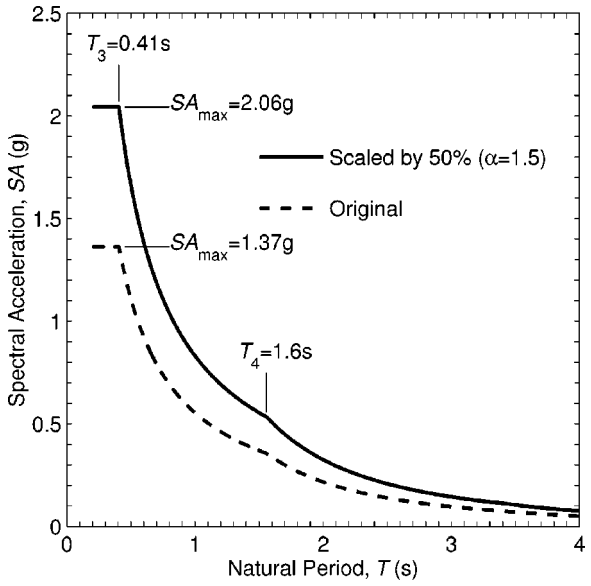

Figure 7. Effect of scaling acceleration history by 50% (α=1.5) on the record's smooth response spectrum.

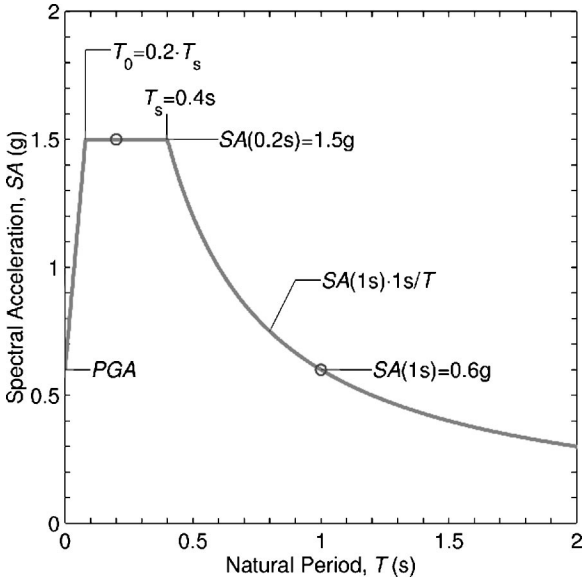

Figure 8. Site-specific response spectrum constructed from spectral values at 0.2 s and 1 s (circles).

Figure 8 shows a 5% damped response spectrum as per the *International Building Code* (ICC 2000) for a site in southern California (Latitude: 34.000°, Longitude: −117.500°), assuming firm rock conditions. This spectrum is constructed from 2475-year return-period spectral values at 0.2 s and 1 s (circles). The control period marking the beginning of velocity region is

$$T_s = 1.0 \text{ s} \cdot \frac{SA(1 \text{ s})}{SA(0.2 \text{ s})} \tag{2}$$

the control period marking the beginning of flat acceleration region is

$$T_0 = 0.2 \cdot T_s \tag{3}$$

and the peak ground acceleration is assumed to be 40% of the spectral value at 0.2 s, i.e.,

$$PGA = 0.4 \cdot SA(0.2s) \tag{4}$$

Unlike spectral values, the duration of strong shaking cannot be read directly from seismic hazard maps. However, we can estimate duration from the size and location of seismic events controlling the hazard at the site. The de-aggregation of seismic hazard (McGuire 1995, Cramer and Petersen 1996, Harmsen and Frankel 2001) reveals the size and location of controlling seismic events.

Figure 9 shows the site-specific de-aggregation plots for 0.2 s, 1 s, and 2 s spectral values downloaded from the USGS web site http://eqint1.cr.usgs.gov/eq/html/deaggint.shtml. Each bar represents a seismic event whose size and distance (from the

(a) *SA*(0.2s)

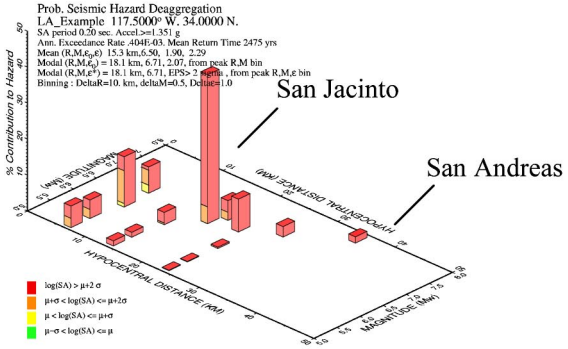

(b) *SA*(1s)

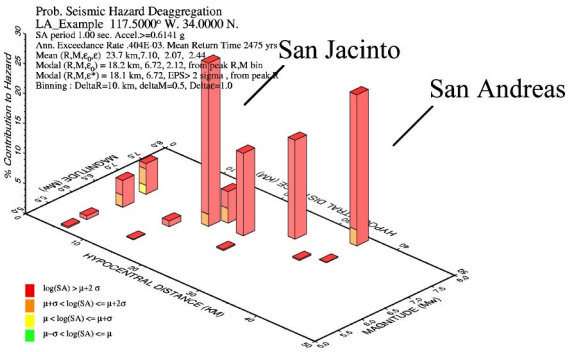

(c) *SA*(2s)

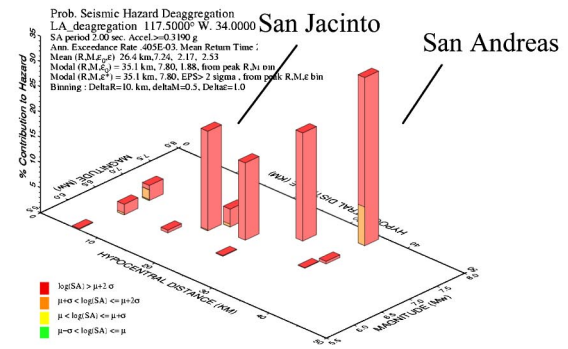

Figure 9. De-aggregation plots for 2475-year spectral values at Latitude: 34.000°, Longitude: −117.500°, from the USGS web site http://eqint1.cr.usgs.gov/eq/html/deaggint.shtml.

site) are indicated along the horizontal axes. The height of the bar signifies the relative importance of a particular seismic event. There are two events that dominate the hazard at this site: (1) $6.7M_w$ at 18 km on the San Jacinto Fault, and (2) $7.8M_w$ at 35 km on the San Andreas Fault.

The 0.2 s spectral value is determined by the San Jacinto event (Figure 9a). The 1 s spectral value is determined, nearly equally, by the San Jacinto and the San Andreas events (Figure 9b). The 2 s spectral value is controlled primarily by the San Andreas event (Figure 9c). The significance of distant event increases with increase in natural period, because low frequencies, which determine the long-period spectral values, attenuate slower with distance than the high frequencies.

The strong-motion durations for the two seismic events are obtained from the following relationship (Trifunac and Brady 1975):

$$D_s = -4.88s + 2.33M + 0.149\Delta \tag{5}$$

where M=earthquake magnitude, Δ=distance from the source, and $s=0$ for alluvium, 2 for hard rock, and 1 otherwise. The duration for the San Jacinto event is $D_s=13$ s, and that for the San Andreas event is $D_s=19$ s. Alternatively, the relationship proposed by Abrahamson and Silva (1996) can be used to estimate the significant duration.

SITE-SPECIFIC GROUND MOTIONS

We need two types of ground motions for this site: (1) those simulating a closer, smaller event on the San Jacinto Fault, and (2) those simulating a distant, larger event on the San Andreas Fault. The ground motions for the closer event should match the site response spectrum for period between 0.2 s and 1 s (Figures 9a and 9b). As mentioned before, these ground motions should have duration of $D_s \approx 13$ s. The ground motions for the distant, larger event should match the site response spectrum for period between 1s and 2s (Figures 9b and 9c) and have duration of $D_s \approx 19$ s. We will select these ground motions from Table 1.

GROUND MOTIONS FOR CLOSER, SMALLER EVENT

We will select those ground motions with $T_3 \approx T_s = 0.4$ s, $T_4 \geqslant 1$ s, and duration $D_s \approx 13$ s. We will scale these ground motions by a factor,

$$\alpha = \frac{SA(0.2s)}{SA_{\max}} \tag{6}$$

The smooth spectra of the scaled ground motions will match the site response spectrum from 0.2 s to 1 s and have the required duration. The Long Valley Dam 0° from the Mammoth Lakes earthquake and the Castaic 90° from the Northridge earthquake are selected, although their durations are somewhat shorter than the target value of 13 s. The $SA_{\max}$ for these ground motions are 0.644 g and 1.37 g, respectively (Table 1). Because

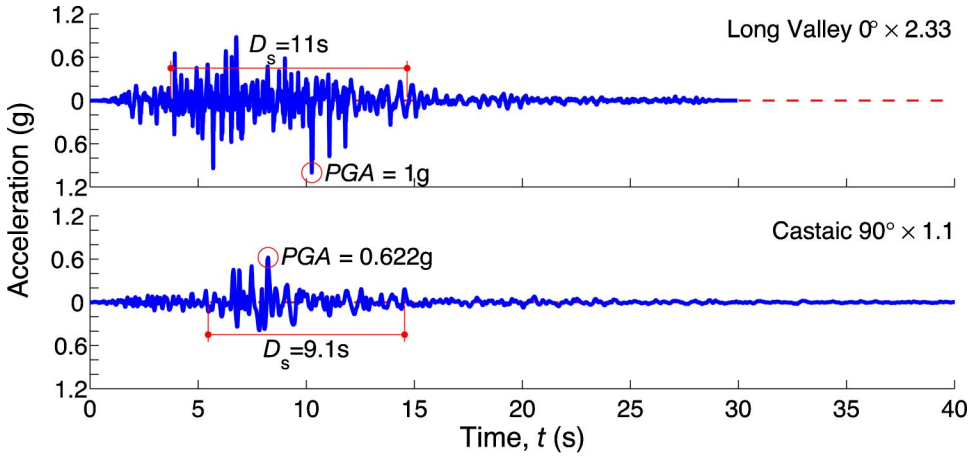

Figure 10. Scaled histories of Long Valley Dam 0° (Mammoth Lakes earthquake) and Castaic Old Ridge Route 90° (Northridge earthquake) ground motions simulating closer, smaller event ground shaking.

SA(0.2 s)=1.5 g, the scaling factors for these ground motions are α=1.5/0.644=2.33 and 1.5/1.37=1.1, respectively. The scaled ground motions are shown in Figure 10. The spectra of the scaled ground motions are compared with the site response spectrum in Figure 11.

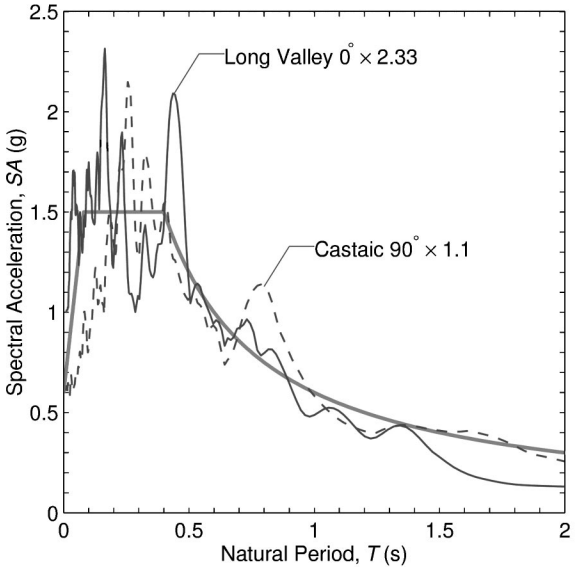

Figure 11. Spectra of closer, smaller event ground motions (Figure 10) compared with the site response spectrum.

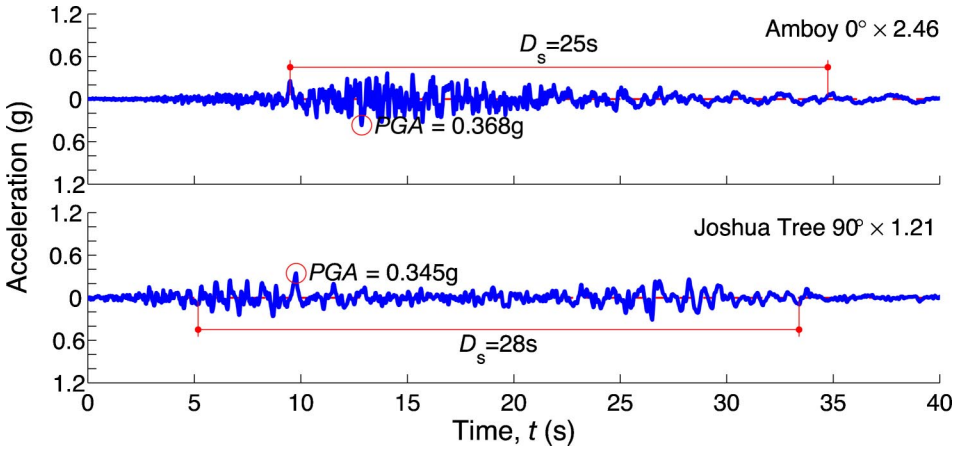

Figure 12. Scaled histories of Amboy 0° (Hector Mine earthquake) and Joshua Tree 90° (Landers earthquake) ground motions simulating distant, larger event ground shaking.

GROUND MOTIONS FOR DISTANT, LARGER EVENT

We will now select ground motions with $T_3 \geqslant 1$ s, $T_4 \geqslant 2$ s, and duration $D_s \approx 19$ s. We will scale these ground motions by a factor,

$$\alpha = \frac{SA(1\ \text{s}) \cdot 1\ \text{s}}{SA_{\max} \cdot T_3} \tag{7}$$

The smooth spectra of the scaled ground motions will match the site spectrum between 1 s and 2 s and have the required duration. The Amboy 0° (Hector Mine earthquake) and Joshua Tree 90° (Landers earthquake) are selected although many other ground motions will also meet the requirements. The scaling factors for these ground motions, as per Equation 7, are 2.46 and 1.21, respectively. The scaled ground motions are shown in Figure 12. The spectra of the scaled ground motions are compared with the site response spectrum in Figure 13.

ORTHOGONAL PAIRS OF GROUND MOTION

In multidirectional dynamic response analyses, the strong-motion records are required in two horizontal directions, simultaneously. The site spectra in two directions are usually the same, but the recorded motions in two orthogonal directions are never identical. It is proposed that the orthogonal pairs of ground motions should be selected such that the geometric mean of their spectra matches the site spectrum and the algebraic mean of their duration matches the required duration.

The Castaic Old Ridge Route 90° ground motion shown in Figure 1 has an orthogonal component in the 0° direction. The spectra of the two orthogonal components are naturally different as shown in Figure 14a. The geometric mean of the Castaic 90° and Castaic 0° spectra is shown in Figure 14b. The smooth geometric-mean spectrum is

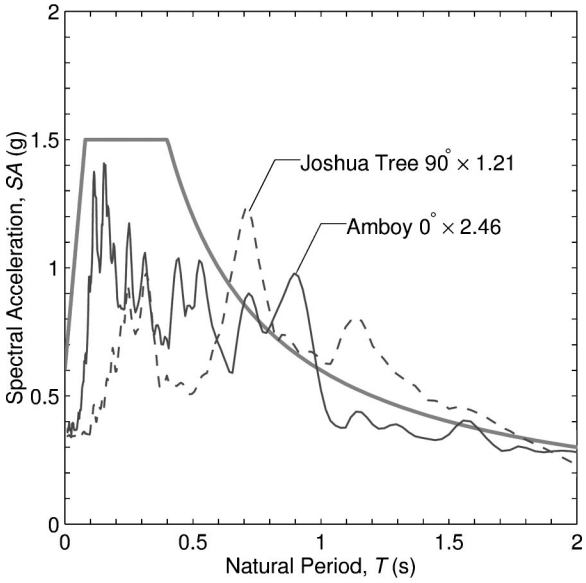

Figure 13. Spectra of distant, larger event ground motions (Figure 12) compared with the site response spectrum.

shown by the solid line in Figure 14b. The smooth geometric-mean spectrum was similarly computed for numerous other ground motion pairs. The parameters defining the geometric-mean spectrum of various horizontal ground motions are listed in Table 2 in the Appendix. The duration shown in the sixth column of Table 2 is the average in the two horizontal directions.

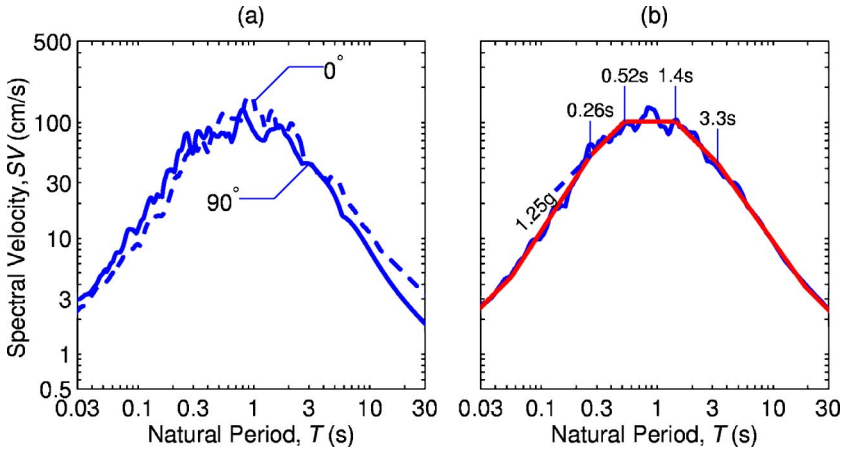

Figure 14. Spectra of two horizontal components of Castaic ground motion from Northridge earthquake: (a) actual spectra of 0° and 90° motions, and (b) geometric mean of 0° and 90° spectra. The smooth geometric-mean spectrum is shown in (b) with the solid line.

The orthogonal pairs of ground motions can be selected from Table 2 using a similar procedure as before. For a closer, smaller event, we need a ground motion pair with $T_3 \approx T_s = 0.4$ s, $T_4 \geq 1$ s, and duration $D_s \approx 13$ s. We will scale both components of this ground motion by the factor given by Equation 6. The Malibu Pt. Dume (Northridge earthquake) ground motion with $SA_{max} = 0.257$ g is selected. It requires a scaling factor of 1.5/0.257=5.84. This factor is higher than the normally accepted upper limit of 4. However, it is still reasonable because we are scaling ground motions to a 2475-year (MCE) spectrum, but the design spectrum as per the *International Building Code* (ICC 2000) is two-thirds the MCE spectrum. This will bring the scaling factor for the design ground motion to 5.84/1.5=3.89, which is within the acceptable limit of 4.

For a distant, larger event, we need a ground motion pair with $T_3 \leq 1$ s, $T_4 \geq 2$ s, and duration $D_s \approx 19$ s. The scaling factor, given by Equation 7, is applied to both components of this ground motion. The Yermo (Landers earthquake) ground motion with $SA_{max} = 0.427$ g and $T_3 = 0.84$ s is selected. It requires a scaling factor of 1.67.

Figure 15 shows the scaled ground motion pairs for the closer, smaller event and the distant, larger event. The geometric-mean spectra of the closer and distant event ground motions are compared with the actual spectrum in Figure 16.

NEAR-FIELD GROUND MOTIONS

Ground motions affected by directivity focusing at near-field stations contain distinct pulses in the acceleration, velocity, and displacement histories (Aki 1968, Archuleta and Hartzell 1981, Bolt 1983). In a strike-slip earthquake, if the rupture propagates in the direction of the recording station, the coherently traveling long-period waves result in large values of ground velocities and displacements (hence medium- and long-period spectral values) in the fault-normal direction (Somerville 1993, 1998). Because the high-frequency waves are less likely to travel in a coherent manner, the ground accelerations (hence low-period spectral values) are relatively unaffected by directivity focusing. Directivity focusing can also occur for dip-slip faulting, although the conditions required are met less readily.

To properly capture the near-field effects different site spectra are needed in the strike-normal and strike-parallel directions (Stewart et al. 2001). In such cases, different scaling factors are applied to the ground motion components to match the respective spectrum. If only one spectrum is available, it may be treated as a geometric-mean spectrum of two orthogonal directions. In this case, ground motion pairs with significantly different spectral amplitudes in two orthogonal directions can be scaled such that their geometric-mean spectrum matches the site spectrum.

Some researchers believe that the ground motions in the fault-normal direction should not only match the site spectrum in that direction, but they should also have a pulse-like characteristic. However, other researchers are of the opinion that the effects of directivity focusing are adequately explained and captured by the response spectrum (Chopra and Chintanapakdee 1998, 2001; Malhotra 1999).

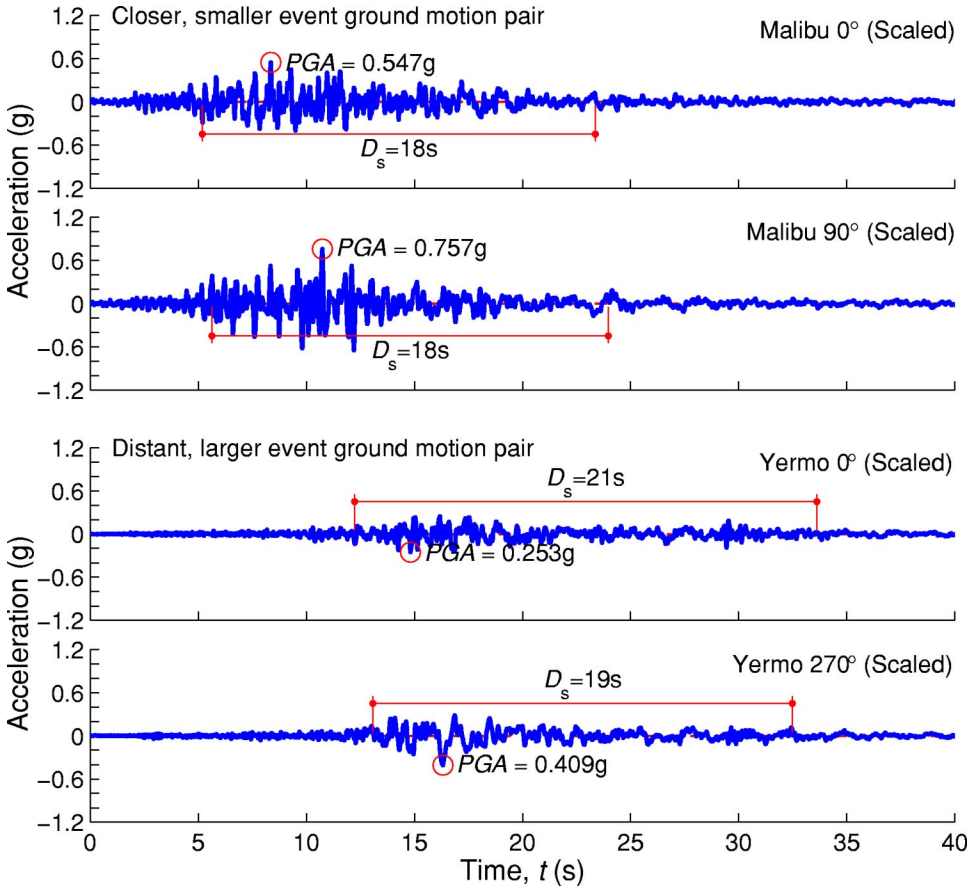

Figure 15. Two orthogonal pairs of scaled ground motions, simulating: (1) closer, smaller event, and (2) distant, larger event.

CONCLUSIONS

1. Site-specific ground motions should simulate the controlling seismic events in amplitude, frequency distribution, and duration. When the site response spectrum is derived from probabilistic hazard analysis, the controlling seismic events can be identified by de-aggregating the hazard.
2. Ground motions simulating closer, smaller events should be compatible with the short-period region of the response spectrum, while those simulating distant, larger events should be compatible with the long-period region of the response spectrum. It is neither necessary nor desirable for a ground motion to be compatible with the entire response spectrum, unless the hazard is controlled by a single seismic event.

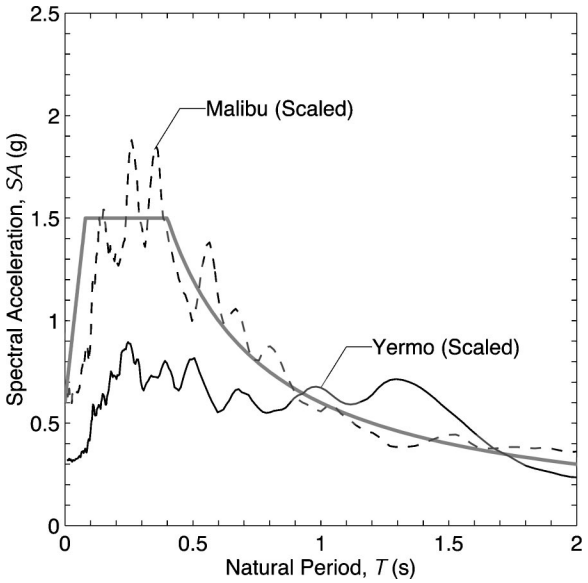

Figure 16. Geometric-mean spectra of two horizontal components of ground motions, simulating closer, smaller event and distant, larger event (Figure 15).

3. The amplitude and frequency distribution of a ground motion are expressed by its smooth response spectrum, which is defined by three parameters: (a) maximum spectral acceleration, (b) period marking the beginning of the velocity region, and (c) period marking the beginning of the displacement region.
4. The tables of amplitude and duration parameters presented in this paper are helpful in selecting strong-motion records for site-specific analysis.

NOTATION

α	amplitude scaling factor (Equations 6 and 7)
D_s	Significant duration (Trifunac and Brady 1975)
M_w	moment magnitude of earthquake
PGA	peak ground acceleration
PGD	peak ground displacement
PGV	peak ground velocity
SA	pseudo-spectral acceleration
SA_{max}	maximum pseudo-spectral acceleration of smooth spectrum (Figures 3 to 5)
SD	spectral deformation (Equation 1)
SV	pseudo-spectral velocity (Equation 1)

T natural period of vibration of structure

T_s period defining the beginning of velocity-sensitive region in site response spectrum (Figure 8)

T_1 to T_6 control periods in smooth spectrum of recorded ground motion (Figure 3)

APPENDIX

The following tables list strong-motion records at various sites for numerous earthquakes. Table 1 gives the amplitude, frequency, and duration parameters for various strong-motion records, and Table 2 gives the amplitude, frequency, and duration parameters for various pairs of horizontal strong-motion records.

Table 1. Amplitude and duration parameters for various strong-motion records

Record (Station & Direction)	Earthquake*	SA_{max} (g)	T_3 (s)	T_4 (s)	D_s (s)	Soil/ Rock	Source of Data**
Taichung–Dajian 90°	Chi-Chi	1.30	0.096	5.57	24	R	COSMOS
Taichung–Dajian 0°	Chi-Chi	1.47	0.113	11.4	19	R	COSMOS
Cape Mendocino 90°	Petrolia	1.93	0.168	3.40	14	R	CSMIP
Site 1 280°	Nahanni, Canada	2.23	0.172	2.69	8	R	PEER
Site 1 10°	Nahanni, Canada	2.32	0.180	1.57	8	R	PEER
Gilroy#3 0°	Loma Prieta	1.73	0.201	1.38	6	S	CSMIP
Mt. Wilson 90°	Sierra Madre	0.601	0.208	0.453	3	R	CSMIP
LA Univ. Hospital 95°	Northridge	0.521	0.217	2.30	13	R	CSMIP
LA City Terrace 90°	Northridge	0.706	0.222	1.54	13	R	CSMIP
San Gabriel 270°	Whittier	0.603	0.223	0.572	8	S	PEER
Cape Mendocino 0°	Petrolia	2.84	0.236	3.91	14	R	CSMIP
Temblor 205°	Parkfield	0.583	0.252	1.60	5	R	PEER
Big Bear Lake 270°	Big Bear	1.18	0.261	0.726	10	R	CSMIP
Whitewater Trout 180°	North Palm Springs	1.58	0.262	0.810	5	R	PEER
Superstition Mtn. 45°	Superstition Hills	1.40	0.271	1.20	12	R	PEER
Big Bear Lake 0°	Big Bear	1.41	0.271	0.611	10	R	CSMIP
Mt. Wilson 0°	Sierra Madre	0.632	0.286	0.511	3	R	CSMIP
LA Baldwin Hills 0°	Northridge	0.605	0.292	2.45	18	R	CSMIP
Olympia WA DOT 270°	Nisqually	0.610	0.297	1.53	17	S	COSMOS
LA City Terrace 0°	Northridge	0.804	0.300	0.885	13	R	CSMIP
Carlo 90°	Denali	0.203	0.300	7.36	25	S	COSMOS
Whitewater Trout 270°	North Palm Springs	1.34	0.301	0.679	3	R	PEER
El Centro Array #1 230°	Imperial Valley	0.280	0.304	7.50	21	S	COSMOS
Temblor 205°	Parkfield	0.642	0.318	0.989	4	R	PEER
Malibu Pt. Dume 90°	Northridge	0.324	0.319	1.94	18	R	CSMIP
Gilroy#1 90°	Loma Prieta	1.14	0.341	1.17	4	R	CSMIP
LA Univ. Hospital 5°	Northridge	1.19	0.350	0.50	11	R	CSMIP
LA Baldwin Hills 90°	Northridge	0.557	0.353	2.90	21	R	CSMIP
Tarzana Cedar Hill 0°	Northridge	2.13	0.363	2.26	13	S	CSMIP
Pacoima Upper Left 104°	Northridge	2.74	0.374	0.496	5	R	PEER
Newhall 90°	Northridge	1.77	0.378	2.04	6	S	CSMIP
Coyote Lake Dam 195°	Morgan Hill	1.58	0.402	0.919	4	R	PEER
Long Valley Dam 0°	Mammoth Lakes	0.644	0.404	1.39	11	R	PEER

Table 1 (cont.). Amplitude and duration parameters for various strong-motion records

Record (Station & Direction)	Earthquake*	SA_{max} (g)	T_3 (s)	T_4 (s)	D_s (s)	Soil/ Rock	Source of Data**
Pacoima Dam Down. 265°	Northridge	0.818	0.406	1.30	4	R	CSMIP
Castaic Old Ridge 90°	Northridge	1.37	0.406	1.56	9	R	CSMIP
LA Temple and Hope 90°	Northridge	0.356	0.408	2.70	16	R	CSMIP
Karakyr 0°	Gazli, Russia	1.46	0.409	4.92	6	S	PEER
Karakyr 90°	Gazli, Russia	1.36	0.413	4.62	7	S	PEER
Long Valley Dam 90°	Mammoth Lakes	0.508	0.416	0.936	11	R	PEER
Tarzana Cedar Hill 90°	Northridge	3.35	0.416	0.843	11	S	CSMIP
Agnews State Hospital 0°	Loma Prieta	0.527	0.416	9.01	25	S	COSMOS
Superstition Mtn. 135°	Superstition Hills	1.51	0.430	0.797	12	R	PEER
Gilroy#2 0°	Loma Prieta	0.874	0.431	1.44	11	S	CSMIP
El Centro Array #1 140°	Imperial Valley	0.299	0.438	9.63	16	S	COSMOS
Arleta Nordhoff Ave. 0°	Northridge	0.684	0.457	3.00	14	S	CSMIP
Bran 0°	Loma Prieta	1.49	0.458	1.03	9	R	PEER
Bran 90°	Loma Prieta	1.35	0.468	0.732	10	R	PEER
Pacoima Dam Down. 175°	Northridge	0.953	0.478	0.795	4	R	CSMIP
Sylmar Hospital 0°	Northridge	2.13	0.491	2.73	5	S	CSMIP
El Centro Array #8 230°	Imperial Valley	0.868	0.499	6.53	6	S	COSMOS
Gilroy#3 90°	Loma Prieta	0.849	0.504	2.65	12	S	CSMIP
El Centro Array #8 140°	Imperial Valley	0.907	0.508	6.37	7	S	COSMOS
Joshua Tree 0°	Hector Mine	0.547	0.516	1.27	13	R	CSMIP
Ahmedabad 78°	Bhuj, India	0.262	0.520	8.49	17	S	COSMOS
Pacoima Kagel Canyon 90°	Loma Prieta	0.739	0.522	2.94	10	R	CSMIP
Carlo 0°	Denali	0.181	0.526	4.15	20	S	COSMOS
Pacoima Upper Left 194°	Northridge	2.35	0.537	0.87	6	R	PEER
Malibu Pt Dume 0°	Northridge	0.221	0.542	1.95	18	R	CSMIP
Yerba Buena Island 0°	Loma Prieta	0.070	0.552	5.16	22	R	CSMIP
EL Centro 0°	El Centro	0.715	0.555	2.52	24	S	COSMOS
Castaic Old Ridge 0°	Northridge	1.24	0.598	1.35	9	R	CSMIP
Petrolia 0°	Petrolia	0.967	0.610	1.37	18	R	CSMIP
Amboy 0°	Hector Mine	0.392	0.622	5.29	25	S	COSMOS
LGPC 90°	Loma Prieta	1.00	0.630	1.63	8	R	PEER
LA Temple & Hope 180°	Northridge	0.428	0.636	0.853	14	R	CSMIP
Olympia WA DOT 180°	Nisqually	0.624	0.637	0.638	20	S	COSMOS
Pacoima Kagel Canyon 0°	Northridge	0.941	0.647	1.13	10	R	CSMIP
Yerba Buena Island 90°	Loma Prieta	0.155	0.662	3.72	8	R	CSMIP
Yermo 0°	Landers	0.416	0.674	8.20	21	S	CSMIP
San Gabriel 180°	Whittier	0.812	0.679	0.681	5	S	PEER
Newhall 0°	Northridge	2.26	0.683	1.54	6	S	CSMIP
Petrolia 90°	Petrolia	1.16	0.731	2.24	16	R	CSMIP
Ahmedabad 348°	Bhuj, India	0.184	0.733	3.06	23	S	COSMOS
Joshua Tree 0°	Landers	0.668	0.736	1.18	31	R	CSMIP
Gilroy#2 90°	Loma Prieta	0.747	0.750	1.59	10	S	CSMIP
Treasure Island 90°	Loma Prieta	0.479	0.750	2.21	5	S	CSMIP
Amboy 90°	Hector Mine	0.416	0.751	5.30	27	S	COSMOS
Rinaldi 318°	Northridge	1.16	0.755	2.68	8	S	CSMIP
Hollister 90°	Loma Prieta	0.473	0.757	6.94	30	S	CSMIP

Table 1 (cont.). Amplitude and duration parameters for various strong-motion records

Record (Station & Direction)	Earthquake*	SA_{max} (g)	T_3 (s)	T_4 (s)	D_s (s)	Soil/ Rock	Source of Data**
Joshua Tree 90°	Landers	0.651	0.759	2.44	28	R	CSMIP
Sylmar Hospital 90°	Northridge	0.993	0.767	3.04	7	S	CSMIP
Arleta Nordhoff 90°	Northridge	0.675	0.794	1.15	13	S	CSMIP
Hollister 0°	Loma Prieta	1.01	0.802	2.35	16	S	CSMIP
University 90°	Kobe, Japan	0.535	0.803	1.78	6	R	PEER
El Centro Array #6 140°	Imperial Valley	0.795	0.811	3.04	11	S	COSMOS
Coyote Lake Dam 285°	Morgan Hill	1.67	0.822	0.824	3	R	PEER
Joshua Tree 90°	Hector Mine	0.288	0.834	1.88	13	R	CSMIP
Agnews State Hospital 90°	Loma Prieta	0.299	0.838	3.46	28	S	COSMOS
LGPC 0°	Loma Prieta	1.38	0.875	3.55	10	R	PEER
Miaoli–Fude School 90°	Chi-Chi	0.309	0.886	12.5	19	R	COSMOS
Rinaldi 228°	Northridge	1.91	0.942	1.26	7	S	CSMIP
Yermo 270°	Landers	0.472	0.946	9.10	19	S	CSMIP
Miaoli–Fude School 0°	Chi-Chi	0.254	0.950	5.80	18	R	COSMOS
Takatori 0°	Kobe, Japan	1.67	0.995	2.24	11	S	COSMOS
Jensen Filter Plant 292°	Northridge	1.51	1.07	1.88	6	R	PEER
Treasure Island 0°	Loma Prieta	0.242	1.08	1.68	6	S	CSMIP
University 0°	Kobe, Japan	0.595	1.13	2.54	7	R	COSMOS
Takatori 90°	Kobe, Japan	1.56	1.15	2.09	10	S	COSMOS
Jensen Filter Plant 22°	Northridge	0.854	1.35	3.63	12	R	PEER
El Centro Array #6 230°	Imperial Valley	0.609	2.40	4.08	8	S	COSMOS

* Bhuj=$7.7M_w$, Big Bear=$6.4M_w$, Chi-Chi=$7.6M_w$, Denali=$7.9M_w$, El Centro=$6.7M_w$, Gazli, Russia =$7.3M_s$, Hector Mine=$7.1M_w$, Imperial Valley=$7.2M_w$, Kobe, Japan=$6.9M_w$, Landers=$7.2M_w$, Loma Prieta=$7M_w$, Mammoth Lakes=$6.1M_w$, Morgan Hill=$6.1M_w$, Nahanni, Canada=$6.9M_w$, Nisqually =$6.8M_w$, North Palm Springs=$6.2M_w$, Northridge=$6.7M_w$, Parkfield=$6.1M_l$, Petrolia=$7M_w$, Sierra Madre=$5.8M_w$, Superstition Hills=$6.7M_w$, Whittier=$6.1M_w$.

** COSMOS=http://db.cosmos-eq.org/
CSMIP=ftp://ftp.consrv.ca.gov/pub/dmg/csmip
PEER=http://peer.berkeley.edu/smcat/

Table 2. Amplitude and duration parameters for various pairs of horizontal strong-motions

Record	Earthquake*	SA_{max} (g)	T_3 (s)	T_4 (s)	D_s (s)	Soil/ Rock	Source of Data**
Taichung–Dajian	Chi-Chi	1.366	0.103	8.812	22	R	COSMOS
Site 1	Nahanni, Canada	2.22	0.175	2.183	8	R	PEER
Mt. Wilson	Sierra Madre	0.404	0.201	0.678	3	R	CSMIP
Cape Mendocino	Petrolia	2.13	0.219	3.96	14	R	CSMIP
LA City Terrace	Northridge	0.820	0.223	1.25	13	R	CSMIP
Gilroy#3	Loma Prieta	1.403	0.229	2.41	9	S	CSMIP
Temblor	Parkfield	0.631	0.274	1.21	5	R	PEER
Gilroy#1	Loma Prieta	0.956	0.289	1.55	5	R	CSMIP
Big Bear Lake	Big Bear	1.37	0.331	0.464	10	R	CSMIP
El Centro Array #1	Imperial Valley	0.293	0.353	9.29	19	S	COSMOS
Whitewater Trout	North Palm Springs	1.39	0.356	0.548	4	R	PEER

Table 2 (cont.). Amplitude and duration parameters for various pairs of horizontal strong-motions

Record	Earthquake*	SA_{max} (g)	T_3 (s)	T_4 (s)	D_s (s)	Soil/ Rock	Source of Data**
LA University Hospital	Northridge	0.796	0.360	0.527	12	R	CSMIP
Tarzana Cedar Hill	Northridge	2.66	0.363	1.577	12	S	CSMIP
LA Baldwin	Northridge	0.511	0.372	2.96	20	R	CSMIP
Carlo	Denali	0.190	0.389	6.51	23	S	COSMOS
Pacoima Upper Left	Northridge	2.58	0.389	0.718	6	R	CSMIP
Karakyr	Gazli, Russia	1.41	0.407	4.13	7	S	PEER
Pacoima Dam Downstream	Northridge	0.857	0.407	1.20	4	R	CSMIP
Malibu Pt. Dume	Northridge	0.257	0.423	2.491	18	R	CSMIP
San Gabriel	Whittier	0.552	0.432	0.676	7	S	PEER
Gilroy#2	Loma Prieta	0.895	0.466	1.79	11	S	CSMIP
Long Valley Dam	Mammoth Lakes	0.557	0.470	0.961	11	R	PEER
LA Temple & Hope	Northridge	0.366	0.494	1.41	15	R	CSMIP
El Centro Array #8	Imperial Valley	0.881	0.508	6.35	7	S	CSMIP
Arleta Nordhoff Ave.	Northridge	0.688	0.519	2.18	14	S	CSMIP
Castaic Old Ridge	Northridge	1.25	0.523	1.43	9	R	CSMIP
Agnews State Hospital	Loma Prieta	0.388	0.558	6.40	27	S	COSMOS
Bran	Loma Prieta	1.31	0.563	0.676	10	R	PEER
Newhall	Northridge	1.62	0.587	1.63	6	S	CSMIP
Sylmar Hospital	Northridge	1.47	0.612	2.42	6	S	CSMIP
Yerba Buena Island	Loma Prieta	0.102	0.613	4.51	15	R	CSMIP
Ahmedabad	Bhuj, India	0.220	0.624	4.089	20	S	COSMOS
Coyote Lake Dam	Morgan Hill	1.536	0.637	0.828	4	R	PEER
Pacoima Kagel Canyon	Northridge	0.813	0.646	1.40	10	R	CSMIP
Olympia WA DOT	Nisqually	0.524	0.661	0.662	19	S	COSMOS
Petrolia	Petrolia	1.04	0.679	1.70	17	R	CSMIP
Amboy	Hector Mine	0.399	0.690	4.83	26	S	CSMIP
LGPC	Loma Prieta	1.17	0.715	2.12	9	R	PEER
Hollister	Loma Prieta	0.653	0.723	5.35	23	S	CSMIP
Rinaldi	Northridge	1.45	0.788	2.12	8	S	CSMIP
Joshua Tree	Hector Mine	0.365	0.823	1.29	13	R	CSMIP
Yermo	Landers	0.427	0.840	8.47	20	S	CSMIP
Miaoli–Fude School	Chi-Chi	0.284	0.859	10.1	19	R	PEER
Joshua Tree	Landers	0.617	0.915	1.36	30	R	CSMIP
Treasure Island	Loma Prieta	0.324	0.949	1.94	6	S	CSMIP
El Centro Array #6	Imperial Valley	0.745	0.960	4.01	10	S	CSMIP
University	Kobe, Japan	0.540	0.976	2.20	7	R	PEER
Jensen Filter Plant	Northridge	1.126	1.09	2.58	9	S	CSMIP
Takatori	Kobe, Japan	1.50	1.27	1.94	11	S	PEER

* Bhuj $=7.7M_w$, Big Bear $=6.4M_w$, Chi-Chi $=7.6M_w$, Denali $=7.9M_w$, El Centro $=6.7M_w$, Gazli, Russia $=7.3M_s$, Hector Mine $=7.1M_w$, Imperial Valley $=7.2M_w$, Kobe, Japan $=6.9M_w$, Landers $=7.2M_w$, Loma Prieta $=7M_w$, Mammoth Lakes $=6.1M_w$, Morgan Hill $=6.1M_w$, Nahanni, Canada $=6.9M_w$, Nisqually $=6.8M_w$, North Palm Springs $=6.2M_w$, Northridge $=6.7M_w$, Parkfield $=6.1M_l$, Petrolia $=7M_w$, Sierra Madre $=5.8M_w$, Superstition Hills $=6.7M_w$, Whittier $=6.1M_w$.

** COSMOS=http://db.cosmos-eq.org/
CSMIP=ftp://ftp.consrv.ca.gov/pub/dmg/csmip
PEER=http://peer.berkeley.edu/smcat/

REFERENCES

Abrahamson, N. A., and Silva, W. J., 1996. Empirical Ground Motion Models, Report to Brookhaven National Laboratory.

Aki, K., 1968. Seismic displacements near a fault, *J. Geophys. Res.* **73** (16), 5359–5376.

Archuleta, R. J., and Hartzell, S. H., 1981. Effects of fault finiteness on near-source ground motion, *Bull. Seismol. Soc. Am.* **71** (4), 939–957.

Bolt, B. A., 1983. The contribution of directivity focusing to earthquake intensities, *Report No. 20*, U.S. Army Corps of Engineers, Vicksburg, MS.

Bommer, J. J., and Martinez-Pereira, A., 1999. The effective duration of earthquake strong motion, *J. Earthquake Eng.* **3** (2), 127–172.

Chopra, A. K., 2001. *Dynamics of Structures: Theory and Applications to Earthquake Engineering* (2nd ed.), Prentice Hall, Englewood Cliffs, NJ.

Chopra, A. K., and Chintanapakdee, C., 1998. Accuracy of response spectrum estimates of structural response to near-field earthquake ground motions: Preliminary results, *ASCE Structures World Conf.*, San Francisco, Paper No. T136-1.

Chopra, A. K., and Chintanapakdee, C., 2001. Comparing response of SDF systems to near-fault and far-fault earthquake motions in the context of spectral regions, *Earthquake Eng. Struct. Dyn.* **30**, 1769–1789.

Cornell, A. C., 1968. Engineering seismic risk analysis, *Bull. Seismol. Soc. Am.* **58** (5), 1583–1606.

Cramer, C. H., and Petersen, M. D., 1996. Predominant seismic source distance and magnitude maps for Los Angeles, Orange and Ventura Counties, California, *Bull. Seismol. Soc. Am.* **86** (5), 1645–1649.

Frankel, A., Mueller, C., Barnhard, T., Perkins, D., Leyendecker, E. V., Dickman, N., Hanson, S., and Hopper, M., 1996. National Seismic Hazard Maps, June 1996 Documentation, *Open File Report 96-532*, U.S. Geological Survey.

Harmsen, S., and Frankel, A., 2001. Geographic deaggregation of seismic hazard in the United States, *Bull. Seismol. Soc. Am.* **91** (1), 13–26.

International Code Council (ICC), 2000. *International Building Code*, Building Officials and Code Administrators International, Inc., Country Club Hills, IL; International Conference of Building Officials, Whittier, CA; and Southern Building Code Congress International, Inc., Birmingham, AL.

Kramer, S. L., 1996. *Geotechnical Earthquake Engineering*, Prentice Hall, Upper Saddle River, NJ.

Krawinkler, H., Zohrei, M., Lashkari-Irvani, B., Cofie, N. G., and Hadidi-Tamjed, H., 1983. Recommendation for experimental studies on the seismic behavior of steel components and materials, *Report No. NSF/CEE-83220*, Stanford University, Stanford, CA.

Leyendecker, E. V., Hunt, R. J., Frankel, A. D., and Rukstales, K. S., 2000. Development of maximum considered earthquake ground motion maps, *Earthquake Spectra* **16** (1), 21–40.

Malhotra, P. K., 1999. Response of buildings to near-field pulse-like ground motions, *Earthquake Eng. Struct. Dyn.* **28** (11), 1309–1326.

Malhotra, P. K., 2001. Response spectrum of incompatible acceleration, velocity and displacement histories, *Earthquake Eng. Struct. Dyn.* **30 (2)**, 279–286.

McGuire, R. K., 1995. Probabilistic seismic hazard analysis and design earthquakes: Closing the loop, *Bull. Seismol. Soc. Am.* **85** (5), 1275–1284.

Newmark, N. M., and Hall, W. J., 1982. *Earthquake Spectra and Design*, Earthquake Engineering Research Institute, Oakland, CA.

Petersen, M., Bryant, W., Cramer, C., Cao, T., Reichle, M., Frankel, A., Lienkaemper, J., McCrory, P., and Schwartz, D., 1996. Probabilistic seismic hazard assessment for the state of California, *Open-File Report 96-08*, California Geological Survey, and *Open-File Report 96-706*, U.S. Geological Survey.

Reiter, L., 1991. *Earthquake Hazard Analysis—Issues and Insights*, Columbia University Press, NY, 254 pp.

Seed, H. B., and Idriss, I. M., 1982. *Ground Motions and Soil Liquefaction During Earthquakes*, Earthquake Engineering Research Institute, Oakland, CA.

Somerville, P., and Graves, R., 1993. Conditions that give rise to unusually large long period ground motions, *Struct. Des. Tall Build.* **2**, 211–232.

Somerville, P. G., 1998. Development of an improved representation of near fault ground motions, *Proceedings SMIP98 Seminar on Utilization of Strong Motion Data*, California Strong Motion Instrumentation Program, Sacramento, CA, pp. 1–20.

Stewart, J. P., Chiou, S. J., Bray, J. D., Graves, R. W., Somerville, P. G., and Abrahamson, N. A., 2001. Ground motion evaluation procedures for performance-based design, *PEER Report 2001/09*, Pacific Earthquake Engineering Research Center, University of California, Berkeley.

Trifunac, M. D., and Brady, A. G., 1975. A study of the duration of strong earthquake ground motion, *Bull. Seismol. Soc. Am.* **65** (3), 581–626.

(Received 7 August 2001; accepted 19 March 2003)